

# Influence of flocculation and coalescence on the evolution of the average radius of an O/W emulsion. Is a linear slope of $\bar{R}^3$ vs. $t$ an unmistakable signature of Ostwald ripening?

German Urbina-Villalba,<sup>\*a</sup> Ana Forgiarini,<sup>b</sup> Kareem Rahn<sup>a</sup> and Aileen Lozsán<sup>a</sup>

Received 29th July 2009, Accepted 16th September 2009

First published as an Advance Article on the web 14th October 2009

DOI: 10.1039/b915470a

The LSW theory of Ostwald ripening, predicts a linear variation of the cube of the average radius of a dispersion as a function of time ( $\bar{R}^3$  vs.  $t$ ) [I. M. Lifshitz, V. V. Slyozov, *J. Phys. Chem. Solids*, 1961, **19**, 35–50; C. Wagner, *Z. Elektrochem.*, 1961, **65**, 581–591]. It also envisages a left-skewed drop-size distribution with a cut-off radius of  $1.5\bar{R}$ . Consequently, non-linear changes of  $\bar{R}^3$  vs.  $t$  are usually ascribed to either a transient period of time (previous to the attainment of the asymptotic limit of ripening) or other destabilisation processes. Up to now the effect of Brownian motion on Ostwald ripening (OR) has not been considered, although it is by far the strongest limitation of the LSW theory. In this work we show the results of incorporating the algorithm of De Smet *et al.* for Ostwald ripening simulations [Y. De Smet, L. Deriemaeker, R. Finsy, *Langmuir*, 1997, **13**, 6884–6888] to our emulsion stability simulations (ESS) code. In particular, the short-time evolution of a dilute dodecane/water nanoemulsion in the absence of stabilisers is studied. At high ionic strength, the simulations suggest that  $\bar{R}^3$  can change linearly with time during the transient period of Ostwald ripening, due to the flocculation and the coalescence of the drops. This behavior is confirmed by the experiments for  $t < 100$  s. At low ionic strength a concave downward curve is observed, both theoretically and experimentally.

## 1. Introduction

According to the theory of Lifshitz–Slyozov–Wagner (LSW), the Ostwald ripening rate  $V_{\text{OR}}$  has a constant value in the asymptotic limit, given by:

$$V_{\text{OR}} = d\bar{R}^3/dt = 4\alpha D_m C(\infty)/9 \quad (1)$$

In the case of an oil (O) in water (W) emulsion,  $\bar{R}$ ,  $D_m$ , and  $C(\infty)$  stand for the average radius of the drops, the diffusion coefficient of the oil molecules and their solubility in the presence of a planar oil/water (O/W) interface. Parameter  $\alpha$ , known as the capillary length, is defined as:

$$\alpha = 2\sigma V_m/\bar{R}T \quad (2)$$

Here:  $\sigma$  is the O/W interfacial tension,  $V_m$  is the molar volume of the oil,  $\bar{R}$  is the universal gas constant, and  $T$  the absolute temperature. Eqn (1) is deduced assuming that the particles are fixed in space and the system is infinitely dilute.

In experiments, the cube of the average radius of an emulsion is often found to vary linearly with time during the asymptotic limit of ripening. However, the value of the ripening

rate is found to be systematically larger than the one predicted by LSW. Oil-in-water emulsions of cyclohexane, *n*-hexane, *n*-octane, *n*-decane, *n*-tetradecane, and *n*-hexadecane, exhibit values of  $V_{\text{OR}}$  which are 32, 97, 679, 8, 3, and 17 times larger than the theoretical prediction.<sup>1</sup> During the transient period, two linear regions with different slopes are usually observed. It is also common to find zones of non-linearity, followed by the characteristic linear dependence.<sup>1–4</sup>

In regard to the form of the drop-size distribution (DSD), right-skewed distributions are far more common than left-skewed ones. Kabalnov *et al.*<sup>5</sup> argued that the surfactant layer could act as a membrane, retarding the molecular diffusion of the oil from the internal phase to the continuous phase, favouring bell-shaped DSDs. Meinders *et al.*<sup>6,7</sup> proposed a connection between the shape of the distribution and the value of the interfacial elasticity.

Schmitt *et al.*<sup>8,9</sup> studied the coarsening of dense alkane/water emulsions stabilised with poly(oxyethylene) surfactants ( $\phi \approx 0.78$ , where  $\phi$  is the volume fraction of oil). After a short period of instability, they found that the initial DSD becomes remarkably narrow, turning to a “wide function” after a certain period of time. The first stage in the evolution of the emulsion was justified in terms of Ostwald ripening, while the second period was mostly characterised by coalescence.

Sakai *et al.*<sup>1,10–12</sup> reported valuable data regarding the evolution of the DSD for several alkane/water systems in the absence of a surfactant. These studies expose the essential features of the Ostwald ripening process related to the oil drops alone. They measured the evolution of a dilute

<sup>a</sup> Instituto Venezolano de Investigaciones Científicas (IVIC), Lab. Fisicoquímica de Coloides, Centro de Física, Carretera Panamericana Km. 11, Aptdo. 20632, Caracas, Venezuela. E-mail: guv@ivic.ve; Fax: (58) 212-5041148

<sup>b</sup> Universidad de Los Andes, Lab. Formulación, Interfaces, Reología y Procesos (FIRP), Fac. de Ingeniería, Ave. Tullio Febres Cordero, Mérida 5101, Venezuela. E-mail: anafor@ula.ve; Fax: (58) 274-2402957

dodecane-in-water emulsion ( $\phi \approx 2.29 \times 10^{-4}$ ) between four minutes and three hours. An OR rate equal to  $4.0 \times 10^{-26} \text{ m}^3 \text{ s}^{-1}$ , three times larger than the theoretical estimation ( $V_{\text{OR}} = 1.3 \times 10^{-26} \text{ m}^3 \text{ s}^{-1}$ ) was determined. All DSDs measured were skewed to the right, contrary to the predictions of LSW.

Using freeze-fracture electron microscopy, Sakai *et al.*<sup>12</sup> also reported direct observations of flocculation and coalescence of metastable benzene droplets in surfactant-free oil-in-water emulsions. Immediately after sonication they observed small drops with diameters at 30–100 nm, and aggregates of medium size (200–500 nm) composed of small droplets. An hour later, the small flocculated drops had coalesced into larger drops. Coalescence of medium size drops was also observed to form large drops (>1000 nm). The benzene drops exhibited a surface potential of  $-35 \text{ mV}$  in the absence of a surfactant.

Because Ostwald ripening mostly depends on the solubility of the oil, while flocculation strongly depends on the repulsive barrier between the drops, it is possible that some variables of these processes can be manipulated in order to favour the occurrence of one process or another. In this regard, it was already shown that the addition of a small amount of insoluble oil (like hexadecane) could retard the process of OR considerably.<sup>11</sup> On the other hand, aggregation can also be delayed adding a suitable surfactant to the dispersion. Thus, it might be possible to observe changes of  $\bar{R}^3$  vs.  $t$  which basically correspond to either OR or to the combined process of flocculation and coalescence (FC). Dilute emulsions, soluble oils, and high surfactant concentrations should favour the rapid attainment of the asymptotic limit of ripening. Sparingly soluble oils and poorly stabilised emulsions should favour the occurrence of flocculation and coalescence previous to a substantial diffusive exchange.

In the present report, new experimental measurements on the short-time evolution of a dodecane-in-water nanoemulsion in the absence of stabilisers are shown. Nanoemulsions were selected in order to disfavour the deformation of the drops. The volume fraction corresponds to the one previously used by Sakai *et al.*<sup>1</sup> However the procedure of preparation of the emulsions is different (see below). Furthermore, the effect of the electrolyte concentration on the stability of the emulsion was also studied. The experimental results are contrasted with novel emulsion stability simulations that include the Ostwald ripening process.

## 2. Theory

### 2.1 Flocculation/coalescence

According to the theory of Smoluchowski,<sup>13</sup> the total number of aggregates in a dispersion decreases as a function of time as a result of irreversible flocculation:

$$n_a = n_0/(1 + k_f n_0 t) \quad (3)$$

Here:  $n_a$  is the total number of aggregates per unit volume, and  $n_0$  the initial number of aggregates ( $n_a(t=0) = n_0$ ). The value of the flocculation rate suggested by Smoluchowski ( $k_s = 4k_B T/3\eta$ ) was corrected afterwards to account for

interactions between the particles:  $k_f = k_s/W$ , where  $W$  is an average stability ratio.

Danov *et al.*<sup>14</sup> demonstrated that eqn (3) also applies to coagulating emulsions, subject to the simultaneous processes of flocculation and coalescence. For this demonstration no distinction was made between the aggregates formed by the collision of smaller clusters, and those of the same size created through the partial coalescence of their flocculated drops. Similarly, non-aggregated particles were regarded as single particles, independently of their size. Hence, no distinction was made between single particles formed through coalescence, and those initially present at  $t = 0$ . Using emulsion stability simulations (ESS) our group confirmed repeatedly the validity of eqn (3) for systems of coalescing non-deformable droplets *whenever* the repulsive potential between the drops is small.<sup>15–18</sup>

The fact that eqn (3) holds for coalescing emulsions is due to the assumptions followed by Smoluchowski for determining the flocculation rate. He pictured the case in which one particle was fixed in space while the others collided with it as a consequence of a gradient of concentration. This gradient was established at time  $t > 0$  between the collision radius of the fixed particle and the bulk of the liquid. The density of particles at the collision radius was kept equal to zero during the whole aggregation process. Hence, the fixed particle acted as a perfect sink. Moreover, the collision efficiency of an aggregate was estimated using the same procedure, but employing the *average hydrodynamic radius* of the cluster, in order to estimate its collision radius. As a result of these assumptions, the theory of Smoluchowski can also be used to follow the change in the total number of aggregates that occur in an emulsion as a consequence of the flocculation and the *coalescence* of drops. This is true if the time required for the coalescence of drops is negligible in comparison to the time required for their flocculation. This is the case of dilute O/W emulsions with an insignificant repulsive potential between their drops.

Previous emulsion stability simulations also showed that eqn (3) is not valid for a flocculating-coalescing emulsion in the presence of a significant repulsive barrier.<sup>15–18</sup> In this case the total number of aggregates changes according to:<sup>15,17</sup>

$$n_a = n_0[A/(1 + k_1 n_0 t) + B \exp(-k_2 n_0 t)] \quad (4)$$

Here,  $k_1$ ,  $k_2$ ,  $A$  and  $B$  are constants, and  $A + B = 1$ . Eqn (4) results from considering flocculation and coalescence as a first order, and a second order reaction, respectively. However, it was shown that  $k_1$  and  $k_2$  contain information on both processes and are not independent of each other.

Eqn (4) describes a combined process in which the number of aggregates decreases sharply at short times as the result of the aggregation and the coalescence of the drops, but progressively stabilises afterwards. This augment of stability at long times results from several phenomena including: (a) a time-dependent surfactant adsorption; (b) the increase of the repulsive forces with the particle radius; (c) the redistribution of surfactant molecules among the interfaces of the drops as the consequence of the progressive decrease in the total surface area of the emulsion; (d) the increase of the mean free path

between the aggregates as the flocculation process evolve, *etc.* All these considerations are valid as long as the drops are non-deformable. When the size of the drops or their aggregates increases considerably ( $R_i > 80 \mu\text{m}$ ), the effects of gravity, drop deformation, and other destabilisation phenomena gain importance, decreasing the stability of the emulsion again.

Whenever the repulsive barrier between the drops is considerably higher than  $13 k_B T^{18}$  (where  $k_B$  is the Boltzmann constant), non-deformable drops behave as solid particles that can flocculate but do not coalesce. In this case, the degree of aggregation depends on the depth of the secondary minimum of the interaction potential between the drops.<sup>19</sup> Profound secondary minima are exhibited by pairs of micron-size drops or larger particles, specially at high ionic strength. Particles of nanometer size exhibit shallow secondary minima or no secondary minima at all. The former particles might show irreversible aggregation and fractal clusters. The latter particles flocculate reversibly or do not aggregate during long periods of time.<sup>17,19</sup>

## 2.2 Emulsion stability simulations

Emulsion stability simulations start from a cubic box that contains  $N$  drops randomly distributed. The particles move with an equation of motion similar to that of Brownian dynamics simulations:

$$\begin{aligned} \vec{r}_i(t + \Delta t) = \vec{r}_i(t) + \left\{ \left( \sum_{\substack{j=1 \\ j \neq i}}^N \vec{F}_{ji} + \vec{F}_{\text{ext}} \right) D_{\text{eff},i}(d, \phi) / k_B T \right\} \Delta t \\ + \sqrt{2D_{\text{eff},i}(d, \phi)\Delta t} [\vec{G}_{\text{auss}}] \end{aligned} \quad (5)$$

According to this equation, the displacement of particle “ $i$ ” during time  $\Delta t$ :  $\vec{r}_i(t + \Delta t) - \vec{r}_i(t)$ , is the result of two contributions. The second term on the right hand side represents deterministic forces, composed of interparticle

$\sum_{i=1, j \neq i}^N \vec{F}_{ji}$  and external forces  $\vec{F}_{\text{ext}}$ , acting on particle  $i$ . The third term on the right hand side of eqn (5) gives the random deviates of the moving particles. The stochastic vector Gauss stands for a set of random numbers, which have a Gaussian distribution with zero mean and unit variance. The characteristic mean square displacement of the Brownian movement is obtained multiplying each random deviate by  $\sqrt{2D_{\text{eff}}(d, \phi)\Delta t}$ .

The attractive potential ( $V_A$ ) is modeled using the formula of Hamaker<sup>20</sup> for the van der Waals interaction ( $V_{\text{vdw}}$ ) between two spherical drops of different radius ( $R_1, R_2$ ):

$$\begin{aligned} V_A = V_{\text{vdw}} = -A_H/12(y/(x^2 + xy + x) \\ + y/(x^2 + xy + x + y)) \\ + 2\ln[(x^2 + xy + x)/ \\ (x^2 + xy + x + y)] \end{aligned} \quad (6)$$

here:  $x = h/2R_1$ ,  $y = R_2/R_1$ ,  $h = r_{ij} - R_1 - R_2$ , and  $r_{ij} = |\vec{r}_i(t) - \vec{r}_j(t)|$ , and  $A_H$  is the Hamaker constant.

In the absence of surfactants, oil drops typically exhibit a small surface potential between  $-10 \text{ mV}$  (octacosane<sup>21</sup>) and  $-35 \text{ mV}$  (benzene<sup>12</sup>) when suspended in water. This electrostatic potential ( $\Psi_0$ ) originates from the preferential adsorption of  $\text{OH}^-$  ions to the oil/water interface.<sup>22,23</sup> It depends on the pH of the solution, the chain length of the hydrocarbon molecules,<sup>22</sup> the size of the drops and the method of preparation of the emulsion. In ESS the value of the surface charge per unit area of the drops ( $\sigma_i$ ) is the result of two contributions. The initial charge of the particles:  $\sigma_0$ , and the additional charge resulting from the adsorption of ionic surfactants to the O/W interface:

$$\sigma_i = \sigma_0 + z_s e N_i^s / (4\pi R_i^2) \quad (7)$$

Here:  $N_i^s$ ,  $z_s$ ,  $e$  and  $R_i$  stand for the number of surfactant molecules attached to drop  $i$ , the effective valence of a surfactant molecule, the unit of electrostatic charge ( $1.6 \times 10^{-19}$  Coulombs), and the radius of particle  $i$ , respectively. In the absence of surfactants either  $\sigma_i = \sigma_0$  or  $\sigma_i = 0$ . If  $\sigma_0 \neq 0$ , the electrostatic potential ( $V_E$ ) contribute to the total interaction potential ( $V_T = V_E + V_A$ ). The program contains several equations to account for the electrostatic potential. According to the formalism of Sader *et al.*:<sup>24,25</sup>

$$V_E/k_B T = (CB(i)B(j)/r_{ij})R_i R_j \exp(-\kappa h) \quad (8)$$

Where:

$$C = 4\pi k_B T \epsilon \epsilon_0 / e^2 \quad (9)$$

$$B(i) = (\Phi_P + 4\bar{\gamma}\Omega\kappa R_i)/(1 + \Omega\kappa R_i) \quad (10)$$

$$\bar{\gamma} = \tanh(\Phi_P/4) \quad (11)$$

$$\Omega = (\Phi_P - 4\bar{\gamma})/(2\bar{\gamma}^3) \quad (12)$$

In eqn (8)–(12),  $\epsilon_0$  is the permittivity of the vacuum,  $\epsilon$  the dielectric constant,  $\kappa^{-1}$  the Debye length, and  $\Phi_P = \Psi_0 e / k_B T$  the reduced electrostatic potential of a particle at its surface. The value of  $\Phi_P$  can be calculated from the numerical solution of eqn (13):

$$\begin{aligned} \sigma_T e / \kappa \epsilon \epsilon_0 k_B T = \Phi_P + \Phi_P / \kappa R_i \\ - \kappa R_i (2 \sinh(\Phi_P/2) - \Phi_P)^2 / \bar{Q} \end{aligned} \quad (13)$$

$$\begin{aligned} \bar{Q} = 4 \tanh(\Phi_P/4) - \Phi_P \\ - \kappa R_i [2 \sinh(\Phi_P/4) - \Phi_P] \end{aligned} \quad (14)$$

Hence, knowledge of  $\sigma_T$  and the ionic strength of the solution allow the evaluation of eqn (8). It is also possible to adjust the value of  $\sigma_T$  in order to reproduce a specific value of  $\Psi_0$ , and calculate the repulsive potential afterwards.

In eqn (5) the forces move each particle with a constant velocity  $\left( \sum_{j=1, j \neq i}^N \vec{F}_{ji} + \vec{F}_{\text{ext}} \right) D_{\text{eff},i}(d, \phi) / k_B T$  during the time step  $\Delta t$ , where  $D_{\text{eff},i}(d, \phi)$  is an effective diffusion constant. In the case of non-deformable particles  $D_{\text{eff},i}(d, \phi)$  is calculated following the methodology described in ref. 26:

$$D_{\text{eff},i}(d, \phi) = D_0 f_{\text{corr}} \quad (15)$$

$$D_0 = k_B T / 6\pi\eta R_i \quad (16)$$

Where  $\eta$  is the shear viscosity of the solvent. At every step of the simulation the space around each particle is divided in three regions. If at least one neighbour particle reaches the internal region of particle  $i$ :  $r_{ij} \leq R_{\text{int}}$  ( $r_{ij} = |\vec{r}_i(t) - \vec{r}_j(t)|$ ,  $d = R_{\text{int}}$ ), the formula of Honig *et al.*<sup>27</sup> is used to correct the diffusion constant of  $i$ . In this case the correction factor of eqn (15),  $f_{\text{corr}}$ , is equal to:

$$f_{\text{corr}} = (6u^2 + 4u)/(6u^2 + 13u + 2) \text{ for } r_{ij} < R_{\text{int}}. \quad (17)$$

Where:  $u = (r_{ij} - R_1 - R_2)/R_R$  and  $R_R$  is a radius of reference. Otherwise the volume fraction of particles around  $i$  is used to evaluate an empirical expression of  $D_{\text{eff},i}(d,\phi)$ :<sup>28,29</sup>

$$f_{\text{corr}} = 1.0 - 1.734\phi + 0.91\phi^2 \quad (18)$$

for  $R_{\text{int}} < r_{ij} < R_{\text{ext}}$ .

In the present simulations  $R_R$  was taken as the average radius of the colliding drops. Particles located at  $r_{ij} > R_{\text{ext}}$  do not contribute to the hydrodynamic interactions of particle  $i$ .

Whenever repulsive forces are present, the change in the number of aggregates as a function of time is calculated at the end of the simulation using an auxiliary code. The co-ordinates of the particles, saved during the simulation run, are used as input. The program analyses the number of neighbours of each particle given a flocculation distance. However, in the absence of a substantial repulsive force, spherical non-deformable drops coalesce as soon as they flocculate. In this case, the change in the number of particles is equal to the change in the number of aggregates.<sup>15</sup>

ESS calculations are very demanding in terms of computer time, limiting the number of particles of the simulations. Previous simulations already showed that a small number of particles ( $N = 125, 216$ ) is enough to calculate an average flocculation rate.<sup>15,16</sup> According to ESS the value of  $k_f$  is equal to  $6.4 \times 10^{-18} \text{ m}^3 \text{ s}^{-1}$  for  $\phi = 10^{-5}$  if the particles interact with an attractive potential, characterised by an effective Hamaker constant ( $A_H$ ) of  $1.24 \times 10^{-21} \text{ Joule}$ .<sup>15</sup> For this estimation, the

particles were allowed to move, flocculate and coalesce according to eqn (5).

A simplified version of the ESS-OR algorithm is shown in Fig. 1 (See ref. 30–32 for details). At the beginning of the simulation the running mode must be specified. The present version of the program has routines for deformable<sup>33</sup> and non-deformable drops, and allows the use of one or two time-steps.

The program can create mono-disperse, Gaussian, Log-normal, LSW, and LSW-like drops size distributions. It can also read the co-ordinates and the size of the particles from an external file. Subsequently, the code distributes the surfactant molecules among the drops and calculates the interfacial parameters. In the case of deformable drops, the interfacial tension of each particle and the initial distance of deformation are calculated at this time. In the case of non-deformable droplets some average diffusion constants depend on the interfacial properties. The formula of Boussinesq<sup>34</sup> for example, depends on the surface viscosity of the drops, which depends in turn on the adsorption of surfactants at the O/W interface.

Following, the forces between the drops can be computed and the particles moved according to eqn (5). The exchange of molecules due to Ostwald ripening proceeds at this point, following the algorithm of De Smet *et al.*<sup>35</sup> (see below). Finally, the program checks for the coalescence of drops. In the case of non-deformable drops coalescence occurs whenever the distance of approach between the drops is smaller than the sum of their radii.

The ESS-OR simulations reported in this work start with  $N(t = 0) = N_0 = 1000$  drops. In a typical ESS, the number of particles decreases progressively until a pre-selected time is reached or only one particle remains in the system. However, in the case of Ostwald ripening a minimum number of particles must be maintained in order to allow for the exchange of oil molecules between the drops. Two different procedures were implemented:

**Procedure A.** The cycle described in Fig. 1 proceeds, while the number of drops is higher than  $N(t = t') = N_1$ . When the number of drops reaches  $N_1$  a new DSD is built with  $N_0$  particles. In the new distribution, the number of particles of radius  $R_i$ ,  $N'(R_i, t = t')$ , is proportional to the number of particles of the same size in the previous distribution  $N(R_i, t = t')$ :

$$\begin{aligned} N'(R_i, t = t') &= N_0(N(R_i, t = t')/N_1) \\ &= N(R_i, t = t')(N_0/N_1) \end{aligned} \quad (19)$$

An auxiliary code calculates the new size of the simulation box, which is required in order to preserve the initial volume fraction of oil with the new set of particles. It also generates a new set of co-ordinates for the new set of 1000 particles. As in the beginning of the simulation, the new particles are distributed at random avoiding overlap. At this point the new DSD is read from a file and the code resumes calculation of the main cycle.

**Procedure B.** The number of particles is allowed to decrease until  $N(t = t') = N_1 = N_0/4$ . At this point, the entire simulation box is translated to the negative quadrant of the coordinate axis, which means that the new coordinates of the

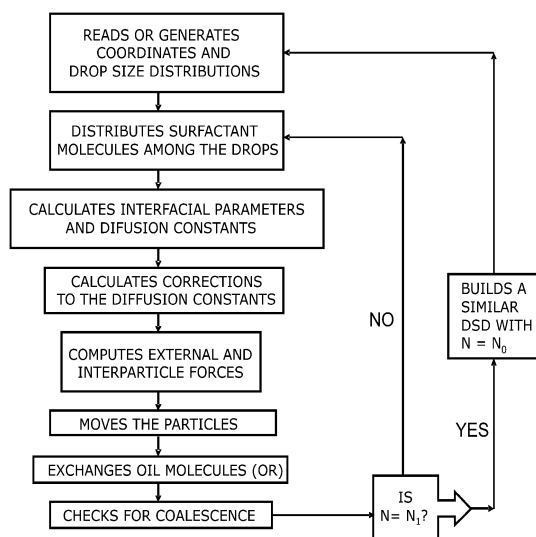


**Fig. 1** Algorithm for Emulsion Stability Simulations with Ostwald ripening included (ESS-OR).

particles are equal to:  $x' = x - L$ ,  $y' = y - L$ ,  $z' = z$  (where  $L$  is the side length of the simulation box). Following, the simulation cell is replicated three times using periodic boundary translations. As a result of this process a rectangular simulation box is created. If  $t'$  refers to the time at which  $N(t = t') = N_1$ , and  $t''$  is taken as the time after which the replication process is over, then for computational purposes  $t'' = t'$ , but:  $L(t'') = 2L(t')$ ,  $V(t'') = 4V(t') = 4V(t = 0)$ ,  $N(t'') = 4N(t = t') = N_0$ ,  $\phi(t'') = \phi(t') = \phi(t = 0)$ , where  $V$  is the volume of the simulation cell. This procedure preserves *exactly* the DSD occurring at  $t = t'$ , as well as the relative coordinates of the set of particles  $N_1$ . Furthermore, it creates three additional sets of particles with the same relative coordinates and particle sizes as the one occurring at  $t = t'$ .

### 2.3 The Ostwald ripening routine

The algorithm of De Smet *et al.*<sup>35</sup> was incorporated to our ESS code in order to simulate the exchange of oil molecules between the drops. The fundamental equation of this method is derived from Fick's law and Kelvin's equation assuming  $\alpha \ll R_i$ :

$$dn_i/dt = 4\pi D_m C(\infty) \alpha (R_{i,k}/R_{c,k} - 1) \quad (20)$$

Here,  $n_i$  stands for the number of molecules of oil in particle  $i$ . Subscript  $k$  identifies the time step of the simulation. Defining:

$$P_{i,k} = R_{i,k}/R_{c,k} - 1 \quad (21)$$

and:

$$M = 4\pi D_m C(\infty) \alpha \Delta t, \quad (22)$$

a simple equation for the exchange of oil molecules is obtained:

$$n_{i,k} = n_{i,k-1} + MP_{i,k} \quad (23)$$

$P_{i,k}$  embodies the growth law. At any time step  $k$  of the simulation, there exists a critical radius  $R_c$ . Particles with  $R_i < R_c$ , dissolve while particles with  $R_i > R_c$  grow. Particles with the same radius as the critical radius  $R_i = R_c$  preserve their size. The number of molecules exchanged by particle  $i$  is equal to the product  $MP_{i,k}$ . The mass balance requires that:

$$\sum P_{i,k} = 0 \quad (24)$$

When the smallest particle  $i = S$  contains fewer molecules than the number it should lose according to eqn (23),  $M$  is substituted by:

$$M_k = n_{S,k}/M \quad (25)$$

Here,  $n_{S,k}$  stands for the number of molecules of particle  $S$  at time step  $k$ . Finsy demonstrated that the critical radius of the LSW theory is equal to the number average radius of the dispersion at each time step:<sup>36</sup>

$$R_{c,k} = \sum_i R_{i,k}/N = \bar{R}_k \quad (26)$$

Prior to the implementation of the Ostwald ripening routine in the ESS code, a standalone OR program was created. In order to distinguish these two programs we will refer to either

ESS-OR or OR programs/calculations, respectively. The OR code matches the algorithm described in ref. 35 (eqn (20)–(26)). Additionally, it has several options for  $M_k$  including  $n_{S,k}/M$ ,  $n_{S,k}$ , and  $n_{S,k}/\sum_i |P_{ik}|$ . When particle  $S$  contains fewer molecules than the number it should lose according to eqn (23), the program has the option to eliminate that particle or preserve it. The OR subroutine of the ESS-OR program exactly matches the one of the separate OR code.

In the OR program, the magnitude of the time step can be fixed arbitrarily large, while in ESS-OR it must be set short enough to sample the interaction potential appropriately. Moreover, in ESS-OR the time step is an input of the simulation. Thus, it enters eqn (22), and determines the amount of molecules that should be transferred by Ostwald ripening according to eqn (23). Hence, the passage of time is unambiguously determined. Instead, the OR code uses  $M$  as input. This variable can be equal to either eqn (22) or (25) depending on the number of molecules of particle  $S$  at step  $k$ . Hence, unlike ESS-OR, the total time  $t_{\text{total}}$  spanned by the OR simulation is not absolute, but proportional to:

$$t_{\text{total}} = \sum_k \Delta t_k \propto \sum_k M_k \quad (27)$$

Yet, the time step used in the OR code can be very large. Thus, this code is very useful to forecast the behaviour of the system at long times, and to establish an approximate time scale for the OR process.

### 3. Computational details

In order to illustrate the differences between the predictions of Ostwald ripening (OR) simulations and emulsion stability simulations with Ostwald ripening included (ESS-OR), two OR-simulations were calculated. These computations correspond to a dodecane-in-water (D/W) nanoemulsion. In both cases the initial drop size distribution (DSD) was Gaussian with an average particle radius  $\bar{R}(t = 0) = \bar{R}_0 = 30$  nm, and a standard deviation of 1.5 nm. The calculations differ in the number of particle sizes used to describe the DSD (see below). In these preliminary simulations a small value of  $M = 0.05$  was selected ( $\Delta t = 5.41 \times 10^{-5}$  s). The parameters corresponding to the Ostwald ripening process were taken from ref. 1:  $D_m = 5.40 \times 10^{-10}$  m<sup>2</sup> s<sup>-1</sup>,  $C(\infty) = 5.31 \times 10^{-9}$  cm<sup>3</sup> cm<sup>-3</sup>,  $\sigma = 52.78$  mN m<sup>-1</sup>,  $V_m = 2.27 \times 10^{-4}$  m<sup>3</sup> mol<sup>-1</sup>.

The main ESS-OR calculations of this work differ from the above computations in three aspects: (1) a much smaller time step is employed:  $2.2 \times 10^{-8}$  s; (2) the methodology of reconstruction of the DSD previously described in section 2.3 is implemented; and (3) the particles move according to eqn (5). In the OR simulations, particles are only lost by dissolution. In the following ESS-OR calculations, the drops can flocculate, coalesce and exchange oil molecules, following the algorithm described in Fig. 1.

The small value of time step chosen for ESS-OR calculations guarantee the appropriate sampling of the potential barriers occurring between the particles. The time span of the present simulations was only a few seconds, very far from the asymptotic limit of ripening predicted by the OR simulations.

The calculations lasted more than 8 months in Dell workstations with Xeon processors of 2.0 GHz.

Four simulations were run. All calculations correspond to dodecane-in-water (D/W) nanoemulsions in the absence of surfactants:

(I) This calculation considered an electrostatic surface potential of  $-19.3$  mV for each drop, in order to account for the adsorption of hydroxyl ions to the oil/water interface. Since this calculation was meant to resemble the evolution of a D/W nanoemulsion in the absence of salt, the ionic strength (I.S.) was set equal to  $10^{-6}$  M NaCl. This produces a long decaying potential with a maximum repulsive barrier of  $10.7$  kT (Fig. 2(b)). Procedure B was employed for the reconstruction of the DSD.

(II) In this calculation the same conditions used for simulation (I) were employed, but the ionic strength was increased to  $0.5$  M NaCl.

(III) This simulation only considered attractive forces between the drops. Procedure A was used for the reconstruction of the DSD, with  $N(t') = N_1 = 200$ .

(IV) In this simulation the possible effect of hydration forces was considered:<sup>37,38</sup>

$$V_{\text{hyd}} = \pi R_i \lambda_0 f_0 \exp(-h/\lambda_0) \quad (28)$$

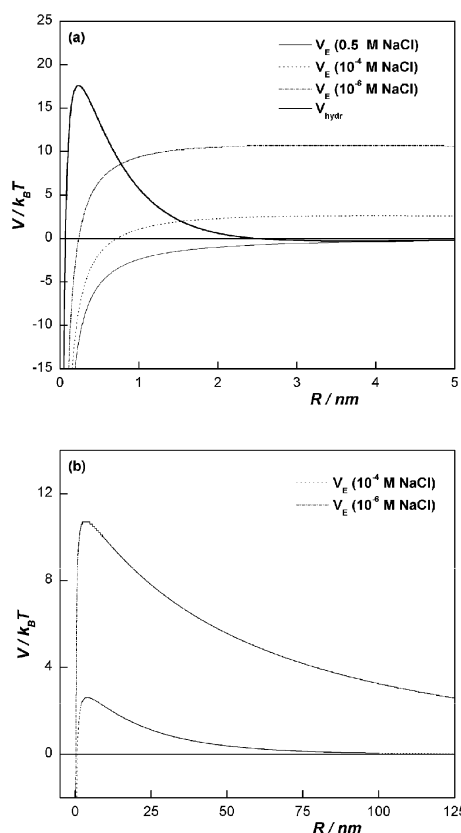


**Fig. 2** Total potential of interaction ( $V_T$ ) between two 30-nm drops of dodecane suspended in water ( $V_T = V_{\text{vdW}} + V_{\text{repulsive}}$ ). Fig. 2(a) shows four curves. The repulsive electrostatic barrier ( $V_{\text{repulsive}} = V_E$ ) decreases with the increase of the ionic strength. For I.S. =  $0.5$  M NaCl, the repulsive barrier is completely screened. The highest repulsive barrier corresponds to the hydration potential ( $V_{\text{repulsive}} = V_{\text{hydr}}$ ), eqn (28). Fig. 2(b) illustrates the long-decaying tail of the electrostatic potential for ionic strengths of  $10^{-4}$  M and  $10^{-6}$  M NaCl.

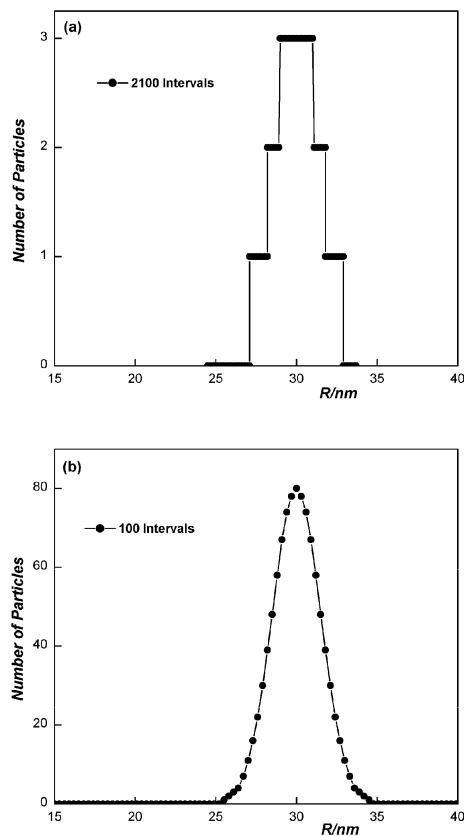


**Fig. 3** Gaussian distributions of particle size obtained for 1000 particles by using (a) 2100 intervals and (b) 100 intervals of particle radii.

with  $\lambda_0 = 0.6$  nm, and  $f_0 = 3$  mJ m $^{-2}$ . This potential is illustrated in Fig. 2(a) along with the potentials of simulations (I) and (II). No electrostatic force was included, and Procedure B was used for the reconstruction of the DSD.

In all cases the initial drop size distribution was selected as Gaussian with an average drop size of 30 nm. For Simulations (I), (II) and (IV) the DSD depicted in Fig. 3(a) was used (see below). In the case of Simulation (III) the DSD illustrated in Fig. 3(b) was employed.

As can be observed in Fig. 2(a), the theoretical electrostatic potential is completely screened by the counterions at I.S. =  $0.5$  M NaCl. Consequently, simulations (II) and (III) should produce the same results except for the effect of the initial DSD and the procedure of reconstruction of the DSD employed.

The value of the Hamaker constant corresponding to two oil drops separated by water was used in all calculations:<sup>39</sup>  $A_H = 5.02 \times 10^{-21}$  J. The effect of retardation was not considered.

## 4. Experimental

### 4.1 Materials

*N*-Dodecane (99% pure) and NaCl (pro-analysis) were obtained from Merck. Water was distilled, deionised (final conductivity  $\lambda_c < 1$   $\mu\text{S cm}^{-1}$ ), and filtered using a Millipore Twin 90 filter with a pore size of  $0.22$   $\mu\text{m}$ .

## 4.2 Emulsion preparation

Dilute dodecane-in-water emulsions were prepared using an Ultraturrax T25 homogenizer at the speed 21 500 rpm during four minutes. A long mixing time was selected in order to obtain a narrow DSD.

## 4.3 Measurements

Immediately after mixing, 2.4 mL of the emulsion were transferred to the measuring cell of a BI-200SM (Brookhaven Instruments) goniometer. Following 0.6 mL of saline solution were quickly injected with the purpose of suppressing the electrostatic potential. The concentration of salt was varied in order to obtain final concentrations of 0 mM, 400 mM and 600 mM in the measuring cell. According to the theoretical expression of the electrostatic potential used, salt concentrations higher than 500 mM are enough to screen the surface charge of the particles completely. However, a minimum concentration of 600 mM of NaCl was found to be necessary in order to produce a slope of  $\bar{R}^3$  vs.  $t$  that did not increase further with the increase of the ionic strength. The final volume fraction of oil in the measuring cell was 1 mM ( $\phi = 2.3 \times 10^{-4}$ ) in all cases.

The light scattered by the sample ( $\lambda = 632.8 \text{ nm}^{-1}$ ) was collected at  $90^\circ$ . The temperature was controlled using a thermostatic bath  $T = 298 \text{ K}$ . The mean diffusion coefficient was derived from the intensity autocorrelation function using cumulant analysis.<sup>40</sup> For technical reasons, the first measurement started at least 6 s after the preparation of the emulsion. A measurement time of 10 s and a sample time of  $1 \mu\text{s}$  was used for all measurements. The total experimental time was limited to 20 min in most cases.

The Z-potential of emulsions drops without added electrolyte was measured three times using a Doppler electrophoresis analyser (Coulter Delsa 440 SX). The measurements were taken approximately five minutes after preparation of the dodecane/water emulsions. The electrostatic potential was found to be  $-35 \text{ mV}$  for an average particle radius of 150 nm.

## 5. Results and discussion

### 5.1 Ostwald ripening simulations without particle movement

The strengths of the OR algorithm proposed by De Smet *et al.* were already illustrated by its authors.<sup>41,42</sup> Some unreported features of this methodology became evident after carrying out an extensive number of simulations using the OR code.

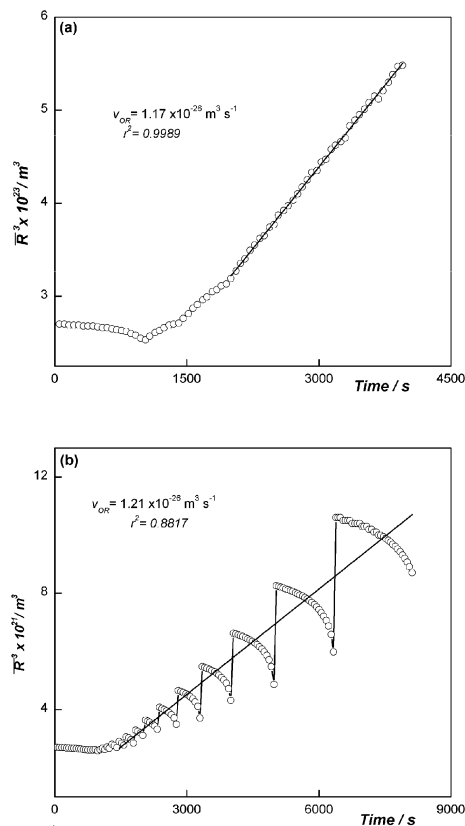
It was found that the allotment of the particle radii along the DSD has a profound influence in the smooth appearance of the DSDs and the  $\bar{R}^3$  vs.  $t$  curves. Furthermore, it was observed that during the transient period of OR, the average particle radius decreases first, passes through a minimum, and then increases. The typical linear increase of  $\bar{R}^3$  vs.  $t$  is only found during the last stage of the process, within the stationary regime.

Since the number of particles of a simulation is finite, the range of particle radii must be divided into intervals in order to build a specific DSD. Either the average value or the limits of

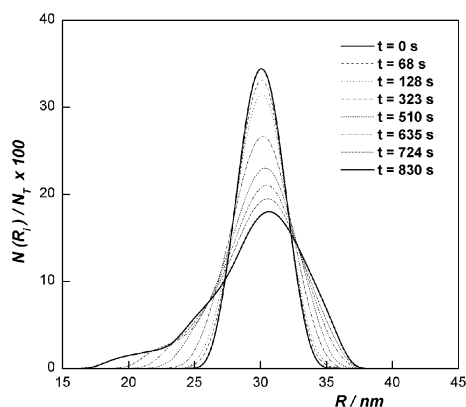
each interval constitute the set of radii selected. The number of particles corresponding to each radius is obtained by multiplying the total number of particles ( $N_0$ ) times the probability of the DSD at this radius. The DSDs illustrated in Fig. 3 correspond to Gaussian distributions with an average particle radius  $\bar{R}(t = 0) = \bar{R}_0 = 30 \text{ nm}$ , and a standard deviation of 1.5 nm. Both distributions were built with 1000 particles. However, the one of Fig. 3(a) required 2100 intervals of particle size while the one of Fig. 3(b) only needed 100 intervals. Inspection of the ordinate axis indicates that there is a substantial number of particles with exactly the same radius in Fig. 3(b), while there are at most three particles with the same radius in Fig. 3(a).

Fig. 4(a) and (b) illustrate the variation of  $\bar{R}^3$  vs.  $t$  in the asymptotic regime calculated with the distributions 3(a) (Calculation A) and 3(b) (Calculation B), respectively.

Analysis of the simulation data shows that the exchange of oil molecules between the particles *decreases* the average particle radius of a Gaussian distribution *at all times*. This explains the negative slope of  $\bar{R}^3$  vs.  $t$  found at short times, as well as the grooves of the saw-tooth variation exhibited by Calculation B (Fig. 4(b)) in the stationary regime. Voorhees and Glicksman<sup>43</sup> already observed this atypical behaviour using a sophisticated population balance approach.



**Fig. 4** Change of  $\bar{R}^3$  vs.  $t$  predicted by Ostwald ripening simulations in the absence of particle movement. The graphs illustrate the evolution of a dilute ( $\phi = 2.29 \times 10^{-4}$ ) dodecane-in-water nanoemulsion in the absence of a repulsive barrier. Fig. 4(a) and (b) correspond to the initial drop size distributions illustrated in Fig. 3(a) and (b), respectively.



**Fig. 5** Evolution of the theoretical drop size distribution predicted by the OR-algorithm<sup>35</sup> for a dodecane-in-water emulsion (D/W).

Augments of the mean particle radius correspond to the elimination of particles. During the transient time, the smaller particles have enough oil molecules to exchange without complete dissolution. As the simulation evolves the smallest particle reaches a point in which it must be eliminated. The increase in the average particle radius of the dispersion due to OR depends on the size and the number of particles eliminated at the same time step  $k$ . The smaller the particle that is eliminated the more linear the curves of  $\bar{R}^3$  vs.  $t$  that are obtained. The smaller the number of particles that are eliminated at the same time step, the smaller the magnitude of the jumps upward in the average particle radius observed in Calculation B. Yet, the average slope of the saw-tooth variation ( $1.22 \times 10^{-26} \text{ m}^3 \text{ s}^{-1}$ ) is similar to the one of Calculation A ( $1.17 \times 10^{-26} \text{ m}^3 \text{ s}^{-1}$ ) which corresponds to the theoretical value of  $V_{\text{OR}}$ .

It is uncertain whether the saw-tooth variation could be observed in practice or it is just an artefact of the OR simulation. Unreported data on  $\bar{R}^3$  vs.  $t$  for a dodecane-in-water emulsion stabilized with Brij30 shows some resemblance with Fig. 4(b). In any event, it is clear from inspection of Fig. 3 and 4 that the specific form of the initial DSD is critical because it determines the change in the average radius of the distribution when the smallest particles are eliminated. Particles of equal radii at the beginning of the simulation will lose or gain the same number of molecules  $MP_{ik}$ . Thus, they will be eliminated at the same time step, favouring a “jump” in the average particle radius (Fig. 4(b)). As a consequence, the worst Gaussian distribution (Fig. 3(a)) produces the smoother change of  $\bar{R}^3$  vs.  $t$ .

Notice also that according to the results presented in Fig. 4,  $\bar{R}^3$  does not increase due to molecular diffusion prior to 800 s. Moreover, the average radius slightly decreases during this period as the consequence of the exchange of molecules. Hence, any increase of  $\bar{R}^3$  vs.  $t$  prior to  $\sim 800$  s is solely the result of the combined process of flocculation and coalescence (FC).

Fig. 5 shows the evolution of the DSD generated by the OR-simulation. The initially Gaussian distribution changes progressively towards an LSW distribution. Notice that the DSDs produced by an OR algorithm are in all cases left-skewed.

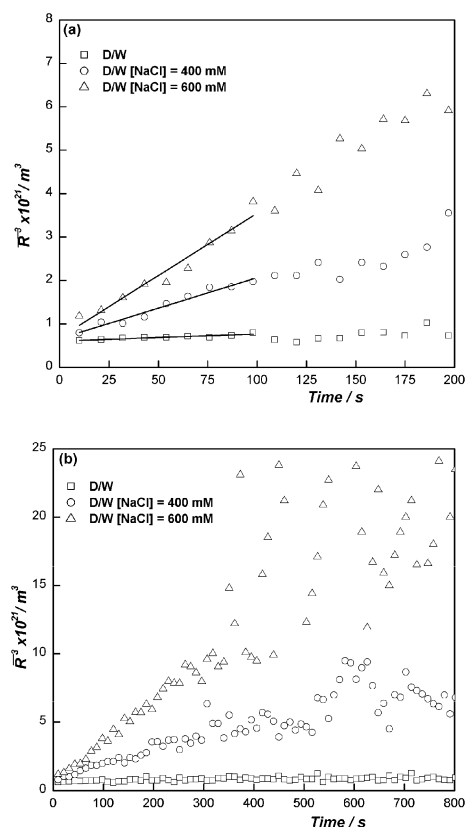


**Fig. 6** Experimental variation of  $\bar{R}^3$  vs.  $t$  for dilute dodecane-in-water (D/W) emulsions. The curves correspond to different concentrations of NaCl: ( $\square$ ) 0 mM, ( $\circ$ ) 400 mM, and ( $\triangle$ ) 600 mM. Fig. 6 (a) shows the linear dependence of  $\bar{R}^3$  vs.  $t$  occurring at short times. Fig. 6(b) shows the long-time variation of  $\bar{R}^3$ .

## 5.2 Emulsion Stability Simulations with Ostwald Ripening included (ESS-OR)

Fig. 6 and 7 show the experimental variation of  $\bar{R}^3$  vs.  $t$  for the D/W emulsions studied. At short times after the preparation of the emulsion ( $t < 100$  s), the variation is apparently linear, showing slopes that depend markedly on the salt

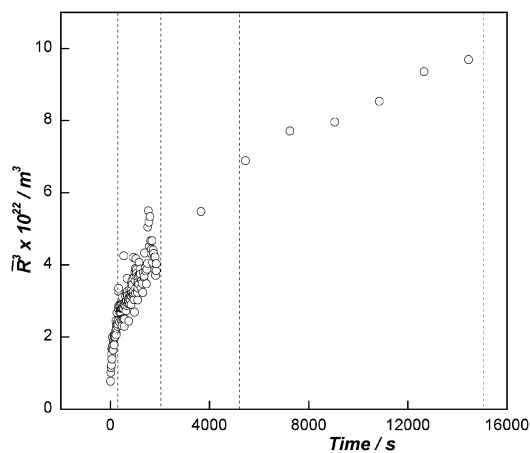


**Fig. 7** Experimental variation of  $\bar{R}^3$  vs.  $t$  for a dilute dodecane-in-water (D/W) emulsion in the absence of salt. For  $t > 20$  min, the sampling time was 30 min.

concentration. Values of  $(1.6 \pm 0.2) \times 10^{-24} \text{ m}^3 \text{ s}^{-1}$  ( $r^2 = 0.8580$ ),  $(1.4 \pm 0.1) \times 10^{-23} \text{ m}^3 \text{ s}^{-1}$  ( $r^2 = 0.9655$ ), and  $(2.9 \pm 0.2) \times 10^{-23} \text{ m}^3 \text{ s}^{-1}$  ( $r^2 = 0.9517$ ) were determined for salt concentrations of 0 mM, 400 mM and 600 mM, respectively.

The dependence of the slope of  $\bar{R}^3$  vs.  $t$  on the ionic strength evidence the substantial surface charge of the dodecane drops. In the absence of surfactants, this charge results from the preferential adsorption of hydroxyl ions to the oil/water interface.<sup>22,23</sup>

At I.S. = 0 mM NaCl, the slope of  $\bar{R}^3$  vs.  $t$  decreases progressively with time, producing a downwards-concave curvature (Fig. 7). The slope of this plot changes from  $(1.6 \pm 0.2) \times 10^{-24} \text{ m}^3 \text{ s}^{-1}$  to  $(3.1 \pm 0.2) \times 10^{-26} \text{ m}^3 \text{ s}^{-1}$  between 6 s and 16 000 s after the preparation of the emulsion. Notice that the initial slope is two orders of magnitude higher than the theoretical value of  $V_{\text{OR}}$ . Furthermore, according to Ostwald ripening simulations, times shorter than 800 s correspond to the transient period of ripening (see Fig. 4). During this period, Ostwald ripening promotes a decrease of  $\bar{R}^3$  as a function of time. However, when the movement of the particles is accounted for (ESS-OR simulations) the initial decrease of  $\bar{R}^3$  vs.  $t$  observed in Fig. 4(a) and (b), does not occur. The rate of flocculation and coalescence (FC) increase the average radius of the emulsion substantially faster than the slight decrease promoted by the Ostwald ripening process during the transient period. Hence

$$d\bar{R}^3/dt = V_{\text{FC}} \quad (29)$$

During this lapse of time, coalescence prevents the elimination of drops due to the generation of larger particles. As the drops grow, their diffusion constant decreases. Moreover, the electrostatic repulsion increases if the surface charge is constant. These two factors slow down the flocculation process, stabilising the DSD. Hence, the FC rate of the process decreases progressively. As a consequence,  $d\bar{R}^3/dt$  changes between  $V_{\text{FC}}$  and  $V_{\text{OR}}$  (Fig. 7) in D/W emulsions in the absence of salt. Consequently, the linear dependence of  $\bar{R}^3$  vs.  $t$  observed for  $t < 100$  s in Fig. 6(a) corresponds to a local slope of the complete curve of  $\bar{R}^3$  vs.  $t$  (Fig. 7).

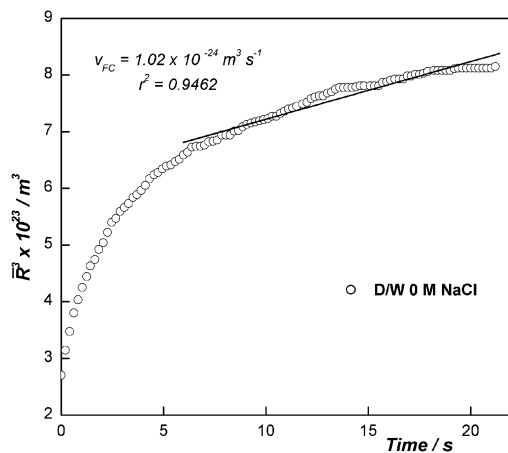


**Fig. 8** Theoretical variation of  $\bar{R}^3$  vs.  $t$  for dilute dodecane-in-water (D/W) emulsions in the absence of salt (Simulation (I)).

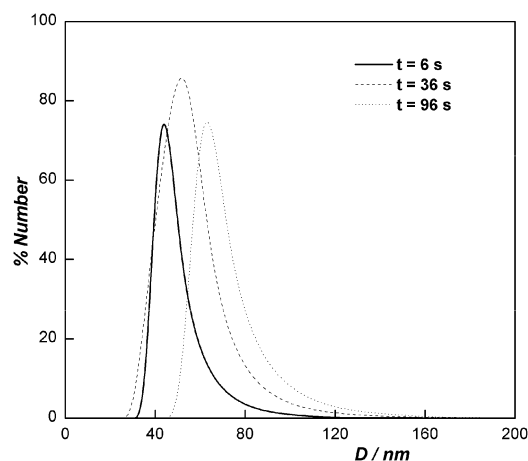


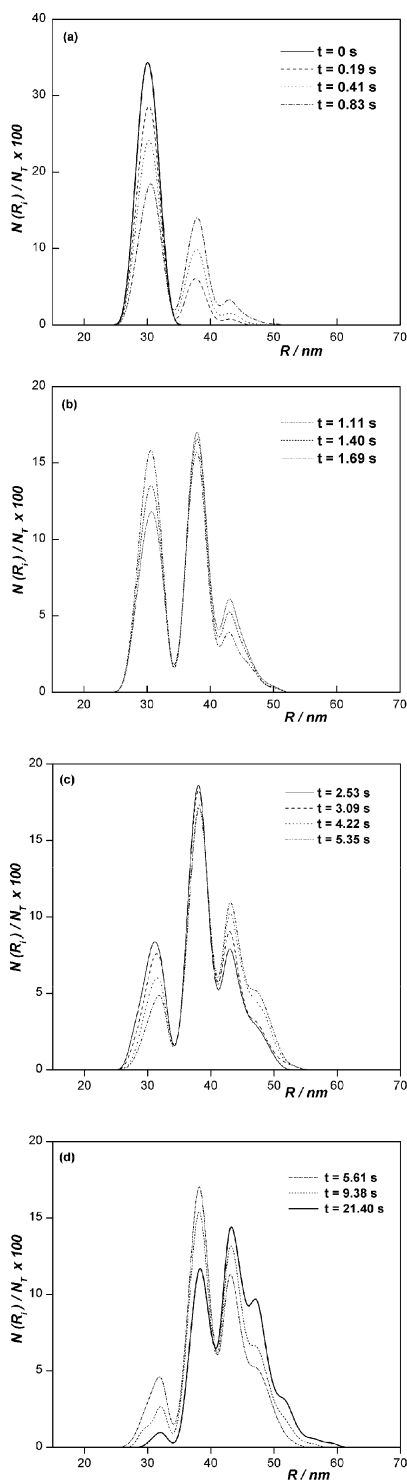
**Fig. 9** Experimental evolution of the drop size distribution for a D/W at I.S. = 0 mM NaCl.

It is important to remark that the final slope of the curve in Fig. 7 is similar to the one reported by Sakai *et al.*:<sup>1</sup>  $3.1 \times 10^{-26} \text{ m}^3 \text{ s}^{-1}$  ( $r^2 = 0.9822$ ). However, this value is three times higher than the theoretical Ostwald ripening rate. Hence, it appears that the discrepancy between the theory and the experiment in regard to the value of  $V_{\text{OR}}$  could be justified in this case in terms of the contribution of flocculation and coalescence to the increase of  $\bar{R}^3$ . Nonetheless, it is observed that the scattering of the experimental data increases considerably after 400 s. The average shape of the curve at long times was obtained, prolonging the time between the measurements after 20 min.

Fig. 8 shows the result of Simulation (I) corresponding to the D/W in the absence of salt. Despite the limited time span of the simulation, a concave-downwards variation similar to the experimental trend is clearly observed. Furthermore, the average slope of the curve between 6 s and 20 s:  $(1.0 \pm 0.5) \times 10^{-24} \text{ m}^3 \text{ s}^{-1}$  ( $r^2 = 0.9462$ ), agrees with the experimental measurement  $(1.6 \pm 0.2) \times 10^{-24} \text{ m}^3 \text{ s}^{-1}$ , within the error bars.

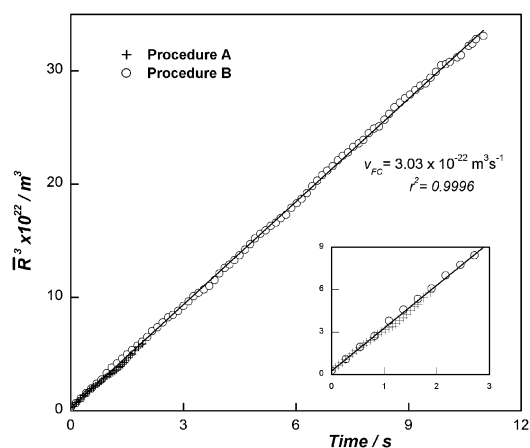
Fig. 9 shows the evolution of the experimental DSD for a D/W emulsion in the absence of salt. The initial DSD measured after 6 s is right-skewed as well as the rest of the distributions up to 16 000 s. Notice that it is not possible to determine the shape of the initial DSD just after the preparation of the emulsion. The evolution of the DSD is fast and it takes a minimum of 6 s to transfer the emulsion from the homogeniser to the measuring cell. In the simulations, the initial distribution was assumed to be Gaussian in order to favor unbiased calculations.

Fig. 10(a)–(d) shows the evolution of the theoretical DSD corresponding to Simulation (I). The Gaussian distribution turns into a right-skewed distribution in a fraction of a second. It is uncertain if all the peaks of the distribution are significant, since the number of particles in the simulation is small, and the histogram is built using an arbitrary discretisation of particle sizes. However, the initial tendency is clear. After the first 2 s further changes of the distribution occur at a considerably slower rate. Between 5 and 10 s the DSD only changes slightly, as if it were possible to reach a stable (self-similar) distribution. In this regard, it should be stressed that the theoretical



**Fig. 10** Theoretical evolution of the DSD for: (a)  $t \leq 0.83$  s, (b)  $1.11 \text{ s} \leq t \leq 1.69$  s, (c)  $2.53 \text{ s} \leq t \leq 5.35$  s, and (d)  $5.61 \text{ s} \leq t \leq 21.40$  s.

estimations of the OR simulations presented on section 5.1, do not take into account the process of coalescence. This process changes the average radius of the emulsion, favoring an increase in the polydispersity that might speed up the OR process. However, no left-skewed DSDs were observed either in the experiments or in the course of the simulations ( $t < 20$  s).



**Fig. 11** Theoretical variation of  $\bar{R}^3$  vs.  $t$  predicted by Simulations (II) and (III) for dilute dodecane-in-water (D/W) emulsions at 0.5 M NaCl.

At high I.S. the situation is different. The experimental curve of  $\bar{R}^3$  vs.  $t$  becomes completely uncorrelated after 300 s (Fig. 6). This could be the result of a large increase in the polydispersity of the emulsion or it could be due to the flocculation of the particles. The volume fraction appears to be somewhat low to account for multiple scattering. In this regard, it was observed that medium-size particles re-appear in the experimental distribution when the vials of the emulsions are gently shaken at the end of the measurements. This indicated the presence of stable flocs that cream. The formation of aggregates delays the increase of the average radius favouring slower  $V_{FC}$  rates. Anyway, it is not possible to establish *experimentally* if the measured value of  $V_{FC}$  corresponds to a local slope of a curve of  $\bar{R}^3$  vs.  $t$  (as in the case of I.S. = 0 M NaCl) or to a more extended linear dependence.

Fig. 11 shows the results of simulations (II) and (III). The results of simulation III correspond to a previous, considerably shorter calculation. Notice that Procedures A and B produce equivalent results.  $V_{FC} = (2.8 \pm 0.1) \times 10^{-22} \text{ m}^3 \text{ s}^{-1}$  ( $r^2 = 0.9959$ ), for Procedure A, and  $(3.031 \pm 0.002) \times 10^{-22} \text{ m}^3 \text{ s}^{-1}$  ( $r^2 = 0.9996$ ) for Procedure B. The comparison between

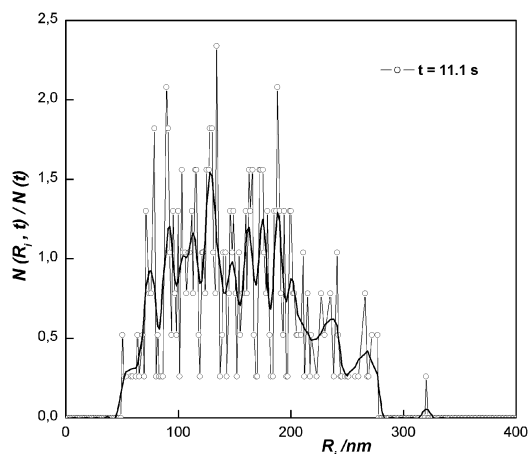


**Fig. 12** Theoretical drop size distribution corresponding to a D/W emulsion at I.S. = 0.5 M NaCl (Simulation (II)).

Fig. 8 and 11 demonstrates that a simulation time of 10 s is enough to distinguish between a non-linear and a linear variation of  $\bar{R}^3$  vs.  $t$ .

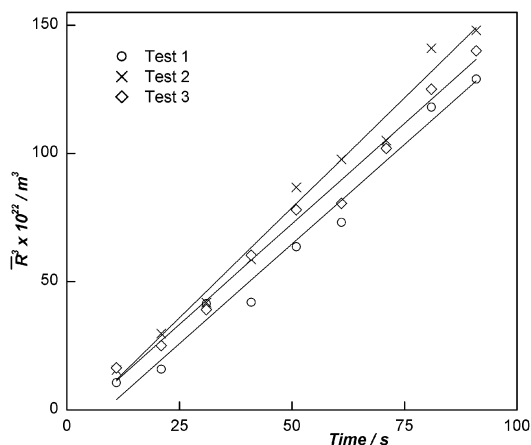
Unlike Simulation (I), the value of  $V_{FC}$  corresponding to simulations (II) and (III) differs in one order of magnitude from the experimental measurement ( $2.9 \times 10^{-23} \text{ m}^3 \text{ s}^{-1}$ ). This indicates that an additional repulsive potential remains after the screening of the electrostatic charge.

Fig. 12 shows the DSD corresponding to Simulation (II). This distribution is highly polydisperse. The number of peaks and the width of the distribution are considerably larger than those observed in Fig. 10. At high salt concentrations, drops larger than 250 nm are observed after 11 s. Instead, a maximum drop size of 60 nm is observed after 26 s in Fig. 10. The stronger destabilization observed for the D/W system in the presence of 0.5 M NaCl is consistent with the experimental results of Fig. 6(b). The destabilisation increases as the ionic strength increases.

It is surprising that despite the considerable polydispersity of the system (Fig. 12),  $\bar{R}^3$  changes linearly with time at high ionic strength. According to this theoretical prediction, it is possible to obtain linear changes of  $\bar{R}^3$  vs.  $t$  as a product of flocculation and coalescence.

In previous reports we had shown that a flocculating-coalescing emulsion follows Smoluchowski's equation (eqn (3)) in the absence of a significant repulsive force.<sup>15–17,32,44</sup> This fact suggested the measurement of  $\bar{R}^3$  vs.  $t$  at high ionic strength for a latex suspension of 96-nm which has been previously studied, both theoretically and experimentally.<sup>44</sup> The Hamaker constant between these latex particles suspended in water was equal to  $4.27 \times 10^{-21}$  J, and the critical coagulation concentration of the suspension was 570 mM. The results of the measurements are shown in Fig. 13. Values of  $(1.55–1.72) \times 10^{-22} \text{ m}^3 \text{ s}^{-1}$  were obtained for  $V_{FC} = V_F$  ( $r^2 = 0.9794$  and  $r^2 = 0.9848$ , respectively). These slopes reproduce the order of magnitude of  $V_{FC}$  suggested by the simulations of D/W at high salt concentrations (Simulation (II)).

The discrepancy between the experimental and the theoretical value of  $V_{FC}$  for D/W emulsions at high ionic strength is puzzling if it is considered that no surfactant is



**Fig. 13** Experimental variation of  $\bar{R}^3$  vs.  $t$  for a latex suspension of 96-nm particles at I.S. = 0.6 M NaCl. The symbols correspond to three different measurements.

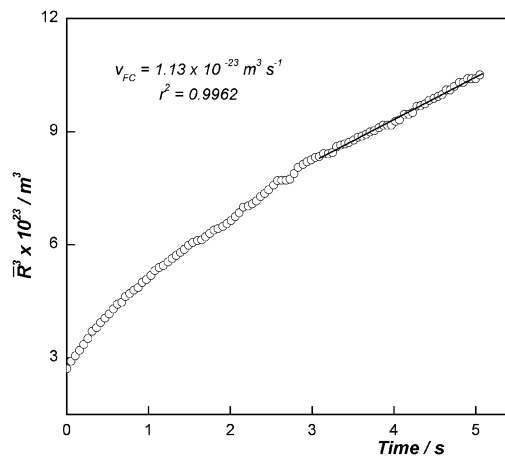


**Fig. 14** Theoretical evolution of  $\bar{R}^3$  vs.  $t$  for a dilute dodecane-in-water (D/W) emulsions taking into account a hydration force.

**Table 1** Rates of change of  $k_f$  and  $V_{FC}$  predicted by ESS-OR for the case of D/W nanoemulsions in the absence of a repulsive barrier

Property/simulation	(II)	(III)
Ionic strength/M	0.5	—
$\bar{R}_0/\text{nm}$	30	30
Potential barrier ( $k_B T$ )	0	0
$k_f \times 10^{18}/\text{m}^3 \text{ s}^{-1}$	7.2, 6.1, 7.3, 7.6	7.4, 7.0
$r^2$	0.9992, 0.9994, 0.9991, 0.9990	0.9944, 0.9991
$V_{FC} \times 10^{22}/\text{m}^3 \text{ s}^{-1}$	3.03	2.83
$r^2$	0.9996	0.9980

present in the system and the electrostatic charge of the drops is completely screened by the high ionic strength. It is clear that a remaining repulsive force is slowing down the FC process.

For the present particle sizes, drop deformation is unlikely. Hence, we considered the effect of hydration on the value of  $V_{FC}$ . According to Israelachvili and Wennerström, this force results from the fluid nature of the O/W interface, and the structural arrangement of the solvent molecules in the region of contact between immiscible phases.<sup>37</sup>

Fig. 14 shows the results of using a hydration force (eqn (28), Fig. 2) as the repulsive force of the simulations. The resulting curve of  $\bar{R}^3$  vs.  $t$  is slightly concave at the beginning, but with a much lower slope than the one exhibit by the D/W system in the absence of salt. The slope of the curve above 3 s comes out to be  $(1.126 \pm 0.003) \times 10^{-23} \text{ m}^3 \text{ s}^{-1}$ . The same order of magnitude as the experimental measurement.

Table 1 shows the flocculation rate of those simulations that conform to Smoluchowski's dynamics (eqn (3)). These rates were calculated from the slope of  $1/n_a$  vs.  $t$ . In the case of Simulation (II) the four cycles of reconstruction of the DSD led to four different values of the flocculation rate. Only two cycles appear in the case of Simulation (III) due to its shorter length. However, in both cases, the complete data of  $\bar{R}^3$  vs.  $t$  produced a single straight line (Fig. 11).

As it was discussed in the introduction, previous works also demonstrated that the evolution of a flocculating/coalescing emulsion follows eqn (4) in a presence of a significant repulsive barrier. Hence, it was found that the data corresponding of Simulation (I) conforms to eqn (4) with:  $A = 0.638 \pm 0.001$ ,

$B = 0.362 \pm 0.001$ ,  $k_1 = (7.66 \pm 0.05) \times 10^{-19} \text{ m}^3 \text{ s}^{-1}$ , and  $k_2 = (5.1 \pm 0.2) \times 10^{-20} \text{ m}^3 \text{ s}^{-1}$  ( $r^2 = 0.9984$ ). For Simulation (IV) the corresponding parameters are:  $A = 0.696 \pm 0.002$ ,  $B = 0.304 \pm 0.002$ ,  $k_1 = (1.16 \pm 0.07) \times 10^{-18} \text{ m}^3 \text{ s}^{-1}$ , and  $k_2 = 5.25 \pm 0.08 \times 10^{-20} \text{ m}^3 \text{ s}^{-1}$  ( $r^2 = 0.9994$ ).

## 6. Conclusions

A novel method of simulation which includes, flocculation, coalescence and Ostwald ripening was described. It is based on emulsion stability simulations and considers the explicit movement of emulsion drops. Special procedures were introduced for the preservation of a minimum number of particles during the simulations. These procedures increase the total number of particles when it reaches a preselected minimum, preserving the shape of the drop size distribution unchanged.

According to the present simulations the entire variation of  $\bar{R}^3$  vs.  $t$  starting from a Gaussian distribution of particle sizes, depends on the repulsive potential between the drops. As the repulsive potential increases, the slope of the curve decreases with time, showing values that range from  $V_{FC}$  to  $V_{OR}$ . At high ionic strength, the simulations predict a linear change of  $\bar{R}^3$  vs.  $t$ . That change occurs during the transient period of ripening and cannot be ascribed to the molecular exchange of oil between the drops. It results from the flocculation and the coalescence of drops.

Moreover, according to ESS-OR calculations, the change in the number of aggregates as a function of time follows Smoluchowski's equation (eqn (3)). The characteristic time of this process  $t_{1/2}$  is of the order of 0.07 s ( $k_f = 7.2 \times 10^{-18}$ ,  $n_0 = 2.0 \times 10^{18}$ ), considerably shorter than the span of the linear variation of  $\bar{R}^3$  vs.  $t$ . Thus, it appears from theoretical considerations that it is possible to obtain a linear variation of  $\bar{R}^3$  vs.  $t$  as a consequence of flocculation and coalescence.

The experimental data corresponding to the dodecane-in-water emulsion at 600 mM NaCl also shows a linear dependence of  $\bar{R}^3$  vs.  $t$  during the first 100 s after the preparation of the emulsion. Such behaviour appears to confirm the theoretical prediction. However the low stability of the emulsion and the increase of the polydispersity as a function of time make it impossible to establish the trend of  $\bar{R}^3$  during a longer period of time (beyond 300 s). Hence, it is uncertain if the linear variation of  $\bar{R}^3$  vs.  $t$  corresponds to a local slope of the curve, or to a genuine linear dependence.

In the absence of salt  $\bar{R}^3$  does not change linearly with time. The slope of the theoretical curve coincides with the one of the experimental determination in the absence of hydration forces. The DSD changes very fast during the first few seconds, and considerably slower afterwards. All the DSD are skewed to the right in contradiction to the LSW prediction. This is due to the effect of flocculation and coalescence during the transient period of ripening.

## References

- 1 T. Sakai, K. Kamogawa, K. Nishiyama, H. Sakai and M. Abe, *Langmuir*, 2002, **18**, 1985–1990.
- 2 Y. De Smet, D. Danino, L. Deriemaeker, Y. Talmon and R. Finsy, *Langmuir*, 2000, **16**, 961–967.
- 3 P. Izquierdo, J. Esquina, Th. F. Tadros, C. Dederen, M. J. García-Celma, N. Azemar and C. Solans, *Langmuir*, 2002, **18**, 26–30.

- 4 J. G. Weers, in *Modern Aspects of Emulsion Science*, ed. B. P. Binks, The Royal Society of Chemistry, London, 1999, ch. 9, pp. 292–325.
- 5 A. S. Kabalnov and E. D. Shchukin, *Adv. Colloid Interface Sci.*, 1992, **38**, 69–97.
- 6 M. B. J. Meinders, W. Kloek and T. van Vliet, *Langmuir*, 2001, **17**, 3923–3929.
- 7 M. B. J. Meinders and T. van Vliet, *Adv. Colloid Interface Sci.*, 2004, **108–109**, 119–126.
- 8 V. Schmitt, C. Cattelet and F. Leal-Calderon, *Langmuir*, 2004, **20**, 46–52.
- 9 V. Schmitt and F. Leal-Calderon, *Europhys. Lett.*, 2004, **67**, 662–668.
- 10 T. Sakai, *Curr. Opin. Colloid Interface Sci.*, 2008, **13**, 228–235.
- 11 K. Kamogawa, M. Matsumoto, T. Kobayashi, T. Sakai, H. Sakai and M. Abe, *Langmuir*, 1999, **15**, 1913–1917.
- 12 T. Sakai, K. Kamogawa, F. Harusawa, N. Momozawa, H. Sakai and M. Abe, *Langmuir*, 2001, **17**, 255–259.
- 13 M. von Smoluchowski, *Z. Phys. Chem.*, 1917, **92**, 129–168.
- 14 K. D. Danov, I. B. Ivanov, T. D. Gurdov and R. P. Borwankar, *J. Colloid Interface Sci.*, 1994, **167**, 8–17.
- 15 G. Urbina-Villalba, J. Toro-Mendoza and M. García-Sucre, *Langmuir*, 2005, **21**, 1719–1728.
- 16 G. Urbina-Villalba, J. Toro-Mendoza, A. Lozsán and M. García-Sucre, *J. Phys. Chem. B*, 2004, **108**, 5416–5423.
- 17 G. Urbina-Villalba, A. Lozsán, J. Toro-Mendoza, K. Rahn and M. García-Sucre, *J. Mol. Struct. (THEOCHEM)*, 2006, **769**, 171–181.
- 18 A. Lozsán, M. García-Sucre and G. Urbina-Villalba, *J. Colloid Interface Sci.*, 2006, **299**, 366–377.
- 19 G. Urbina-Villalba and M. García-Sucre, *Langmuir*, 2005, **21**, 6675–6687.
- 20 H. C. Hamaker, *Physica IV*, 1937, 1058–1072.
- 21 S. R. Reddy, D. H. Melik and H. S. Fogler, *J. Colloid Interface Sci.*, 1981, **82**, 117–127.
- 22 J. Stachurski and M. Michalek, *J. Colloid Interface Sci.*, 1996, **184**, 433–436.
- 23 K. G. Marinova, R. G. Alargova, N. D. Denkov, O. D. Velez, D. N. Petsev, I. B. Ivanov and R. P. Borwankar, *Langmuir*, 1996, **12**, 2045–2051.
- 24 J. E. Sader, *J. Colloid Interface Sci.*, 1997, **188**, 508–510.
- 25 M. R. Oberholzer, J. M. Stankovich, S. L. Carnie, D. Y. C. Chan and A. M. Lenhoff, *J. Colloid Interface Sci.*, 1997, **194**, 138–153.
- 26 G. Urbina-Villalba, M. García-Sucre and J. Toro-Mendoza, *Phys. Rev. E: Stat., Nonlinear, Soft Matter Phys.*, 2003, **68**, 061408.
- 27 E. P. Honig, G. J. Roeberson and P. H. Wiersema, *J. Colloid Interface Sci.*, 1971, **36**, 97–109.
- 28 C. W. J. Beenakker and P. Mazur, *Phys. Lett. A*, 1982, **91**, 290–291.
- 29 W. van Megen, S. M. Underwood, R. H. Ottewill, N. St. J. Williams and P. N. Pusey, *Faraday Discuss. Chem. Soc.*, 1987, **83**, 47–47.
- 30 G. Urbina-Villalba and M. García-Sucre, *Langmuir*, 2000, **16**, 7975–7985.
- 31 G. Urbina-Villalba, J. Toro-Mendoza, A. Lozsán and M. García-Sucre, in *Emulsions: Structure, Stability and Interactions*, ed. D. N. Petsev, Elsevier Ltd., Amsterdam, 2004, ch. 17, pp. 677–719.
- 32 G. Urbina-Villalba, *Int. J. Mol. Sci.*, 2009, **10**, 761–804.
- 33 J. Toro-Mendoza, PhD Thesis, IVIC, 2008.
- 34 J. Boussinesq, *C. R. Acad. Sci.*, 1913, **156**, 1124–1129.
- 35 Y. De Smet, L. Deriemaeker and R. Finsy, *Langmuir*, 1997, **13**, 6884–6888.
- 36 R. Finsy, *Langmuir*, 2004, **20**, 2975–2976.
- 37 J. N. Israelachvili and H. Wennerström, *J. Phys. Chem.*, 1992, **96**, 520–531.
- 38 I. B. Ivanov, K. D. Danov and P. A. Kralchevsky, *Colloids Surf., A*, 1999, **152**, 161–182.
- 39 D. B. Hough and L. R. White, *Adv. Colloid Interface Sci.*, 1980, **14**, 3–41.
- 40 R. T. C. Ju, C. W. Frank and A. P. Gast, *Langmuir*, 1992, **8**, 2165–2171.
- 41 K. N. Hoang, L. Deriemaeker, V. B. La and R. Finsy, *Langmuir*, 2004, **20**, 8966–8969.
- 42 T. K. N. Hoang, V. B. La, L. Deriemaeker and R. Finsy, *Langmuir*, 2002, **18**, 10086–10090.
- 43 P. W. Voorhees and M. E. Glicksman, *Acta Metall.*, 1984, **32**, 2013–2030.
- 44 G. Urbina-Villalba, A. Lozsán, K. Rahn and M. S. Romero-Cano, *Comput. Phys. Commun.*, 2009, **180**, 2129.